Discovery of 14-3-3 PPI Stabilizers by Extension of an Amidine-Substituted Thiophene Fragment

ChemBioChem

Research Article
doi.org/10.1002/cbic.202300636

Chemistry Europe
European Chemical Societies Publishing

www.chembiochem.org

Special Collection

Discovery of 14-3-3 PPI Stabilizers by Extension of an Amidine-Substituted Thiophene Fragment

Qi Wu[+],[a] Federica Centorrino[+],[a] Xavier Guillory,[a] Madita Wolter,[a] Christian Ottmann,*[a] Peter J. Cossar,*[a] and Luc Brunsveld*[a]

Protein-protein interaction (PPI) modulation is a promising approach in drug discovery with the potential to expand the 'druggable' proteome and develop new therapeutic strategies. While there have been significant advancements in methodologies for developing PPI inhibitors, there is a relative scarcity of literature describing the 'bottom-up' development of PPI stabilizers (Molecular Glues). The hub protein 14-3-3 and its interactome provide an excellent platform for exploring conceptual approaches to PPI modulation, including evolution of chemical matter for Molecular Glues. In this study, we employed a fragment extension strategy to discover stabilizers for the complex of 14-3-3 protein and an Estrogen Receptor alpha-derived peptide (ERα). A focused library of analogues derived from an amidine-substituted thiophene fragment enhanced the affinity of the 14-3-3/ERα complex up to 6.2-fold. Structure-activity relationship (SAR) analysis underscored the importance of the newly added, aromatic side chain with a certain degree of rigidity. X-ray structural analysis revealed a unique intermolecular π–π stacking binding mode of the most active analogues, resulting in the simultaneous binding of two molecules to the PPI binding pocket. Notably, analogue **11** displayed selective stabilization of the 14-3-3/ERα complex.

Introduction

The modulation of protein-protein interactions (PPIs) has vastly expanded the 'druggable' proteome.[1] The methodologies to develop PPI inhibitors are now well established, with next to high-throughput screening (HTS), for example, fragment-based drug discovery (FBDD) approaches to identify molecular starting points.[2] These approaches frequently identify small molecule PPI inhibitors that mimic pharmacophoric features of a peptide epitope, such as an α-helix of an interacting protein partner, enabling the direct competition for the PPI interface.[3] Venetoclax, for instance, in this manner effectively inhibits the Bcl-2/Bax interaction, triggering apoptosis in tumor cells.[4] In contrast, stabilizing or inducing PPIs represents an intriguing converse strategy to tackle therapeutic challenges. This concept of bringing proteins together with molecular glues[5] is the basis of the immunomodulatory drugs (IMiDs) and related breakthrough PROteolysis TArgeting Chimeras (PROTACs) which bridge an E3 ligase and a target protein to achieve protein degradation.[6] However, the literature sparsely describes 'bottom-up' design and development of PPI stabilizers, with most molecular glues discovered by serendipity.[7]

The hub protein 14-3-3 provides an excellent training ground for the development of novel approaches to the 'bottom-up' identification of molecular glues – owing to the deep composite pocket formed by 14-3-3 and its partner protein, upon complex formation, which in turn enables simultaneous engagement of molecular glues with both proteins of the complex.[8] The natural products fusicoccanes (FCs) and their semi-synthetic analogues have been shown to stabilize several 14-3-3-based PPIs including 14-3-3/ERα,[9] 14-3-3/Task3,[10] 14-3-3/CFTR,[11] 14-3-3/p65[12] by binding in the composite interfacial pocket defined by the specific PPI complex.

Several hundred 14-3-3 interaction partners have been described in the literature.[13] Among those, numerous disease-relevant proteins have been identified, including the Hippo pathway transcription factors YAP and TAZ,[14] the tumor suppressor p53,[15] and the Raf kinases.[16] The vast 14-3-3 interactome and its implication in various human diseases make it a valuable target for drug development, offering potential opportunities to treat a wide range of disease conditions. 14-3-3 exerts its function chiefly by binding to disordered regions of partner proteins, typically via interactions with phosphorylated binding motifs, modulating the partner protein's enzymatic activity, subcellular localization, or acting as scaffolding protein.[17] However, the vast complexity of the 14-3-3 interactome poses a challenge in selectively modulating specific 14-3-3 protein-protein interactions. While fusicoccanes

[a] *Q. Wu,[+] Dr. F. Centorrino,[+] Dr. X. Guillory, Dr. M. Wolter, Dr. C. Ottmann, Dr. P. J. Cossar, Dr. L. Brunsveld*
Laboratory of Chemical Biology
Department of Biomedical Engineering and
Institute for Complex Molecular Systems
Eindhoven University of Technology
P.O. Box 513, 5600 MB Eindhoven (The Netherlands)
E-mail: c.ottmann@tue.nl
p.cossar@tue.nl
l.brunsveld@tue.nl

[+] *These authors contributed equally to this work.*

Supporting information for this article is available on the WWW under https://doi.org/10.1002/cbic.202300636

This article is part of the Special Collection: Celebrating 120 Years of the Royal Netherlands Chemical Society (Koninklijke Nederlandse Chemische Vereniging).

are available as potent, and in part selective, molecular glues for 14-3-3 PPIs, their chemical complexity has hampered their further development as therapeutic agents.

Previously, our research group and colleagues have shown that the composite binding pockets shaped collectively by the amphipathic groove of 14-3-3 and the phospho-client peptides can be targeted using synthetic small molecules.[18] For example, by establishing a customized interaction involving π–π stacking between the aldehyde fragments and a critical Trp residue in the Pin-1 phospho-client peptide, selective stabilization of the 14-3-3/Pin-1 complex was achieved.[18b] Most of these examples deal with fragments bound via dynamic covalent chemistries. Recent examples of synthetic non-covalent 14-3-3 PPI Molecular Glues highlight the potential of further exploring strategies for chemical maturation of non-covalent fragment libraries.[19]

Here, we performed non-covalent fragment extension as a previously non-addressed concept for 14-3-3 PPI stabilization. Specifically, in this fragment extension approach we explored the potential to build off from a non-covalent amidine substituted thiophene fragment (Figure 1B).[18c] A focused library of analogues was synthesized and evaluated for their effect on the stability of the 14-3-3/ERα complex. Through fluorescence anisotropy (FA) assays and X-ray crystallography, we determined the stabilization effect of the analogues and established a first structure-activity relationship (SAR). Notably, we identified a unique π–π stacking binding mode of the most active analogues, yielding simultaneous binding of two molecules in the composite PPI binding pocket. Additionally, we demonstrated the selective stabilization of 14-3-3/ERα complex over other PPIs using the best analogue.

Results and Discussion

Chemistry

In our previous crystallography-based fragment screening, we discovered a hit fragment, 5-methyl-4-phenylthiophene-2-amidine (**AZ-017**),[18c] which sits on a 14-3-3 molecular cushion formed by E39, N42, and L43 in the vicinity of the composite binding pocket of the 14-3-3/p53pT387 complex.[18c] Upon inspection of the co-crystal structural superposition of the 14-3-3/p53pT387/AZ-017 (PDB: 6SIO) ternary complex and the 14-3-3/ERα (PDB: 4JC3) binary complex, we observed that the ERα molecular elements are in proximity to the binding site of **AZ-017** (Figure 1B, p53pT387 not shown), suggesting the potential for establishing contacts by extension of the fragment. To explore this potential, we initiated a fragment growing campaign, focusing on position C-5 of the thiophene core, as this vector aligns with the gap between **AZ-017** and the ERα peptide. We designed a divergent synthetic route to generate a library of analogues. This route involves employing amide coupling to introduce commercially available carboxylic acids onto the fragment scaffold. 5-methylthiophene-2-carbaldehyde (**1**) was selected as the starting material due to its commercial availability and the ease of functionalizing the methyl group (Scheme 1).

Critical to the synthesis of the library was the synthesis of advanced amine intermediate **7**. Synthesis of **7** began with the bromination of commercially available 5-methylthiophene-2-carbaldehyde (**1**) using elemental bromine and acetic acid affording a mixture of C-3 and C-4 regioisomers (**2**). Without further purification, the mixture underwent a one-pot nucleophilic addition/dehydration cascade, resulting in the formation of isomeric nitrile (**3**). The obtained isomers were then subjected to a Suzuki coupling reaction, yielding a single product **4** with phenyl ring installed at C-4 position as determined by Heteronuclear Multiple Bond Correlation (HMBC) measurement (Figure S1). According to the HMBC spectrum, long range ^{1}H-^{13}C coupling between the hydrogen atom

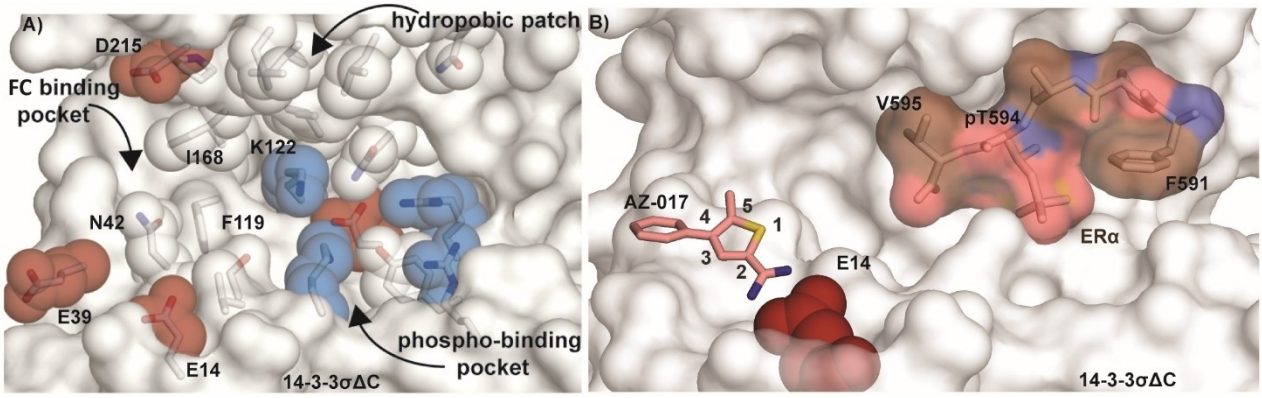

Figure 1. Structural analysis of the 14-3-3 binding groove and structural model of **AZ-017** bound to 14-3-3/ERα complex. (A) Detailed view of the amphipathic 14-3-3 binding groove. Hydrophobic and polar amino acids are depicted with grey sticks and spheres, charged amino acids are represented with red or blue sticks and spheres. The black arrows highlight the phospho-binding pocket, the fusicoccane binding pocket, and the cluster of hydrophobic residues of the groove. (B) Fragment **AZ-017** (pink sticks) modelled in co-crystal structure of 14-3-3 (white surface) and ERα (colored surface) by structural alignment of 14-3-3/p53pT387/AZ-017 ternary co-crystal structure (PDB: 6SIO) with 14-3-3/ERα binary co-crystal structure (PDB: 4JC3). p53pT387 is not shown in the structure. Position 5 of the thiophene core of the fragment shows promise for extension to make contact with ERα.

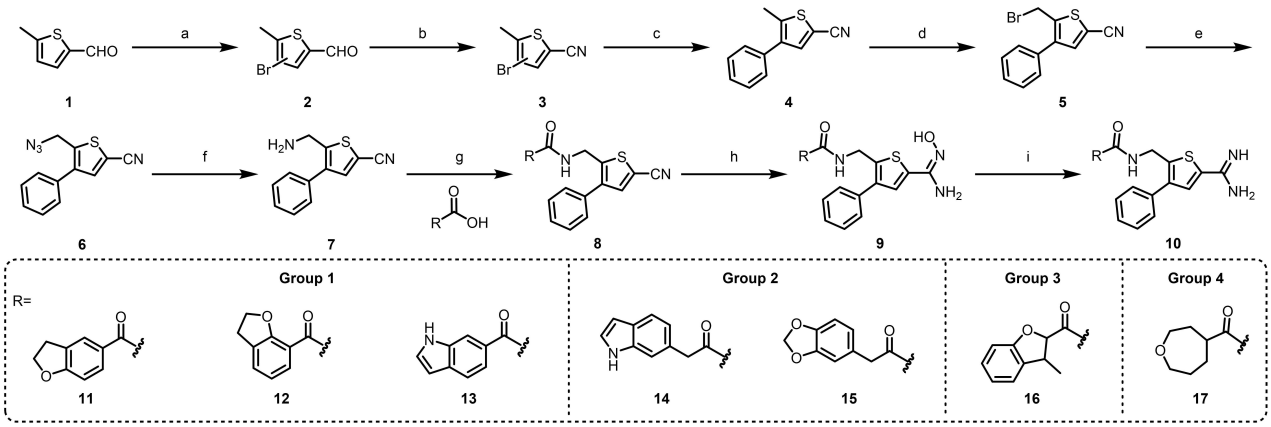

Scheme 1. Synthesis of analogues **11**–**17**. Reagents and conditions: (a) Br_2, AcOH, 0 °C to rt, 40 %; (b) $NH_2OH \cdot HCl$, CuO, AcONa, reflux, 75 %; (c) $PhB(OH)_2$, $Pd(PPh_3)_4$, Na_2CO_3, DME, Ar, 80 °C, 60 %; (d) NBS, BPO, DCE, reflux, 90 %; (e) NaN_3, Acetone, rt, 76 %; (f) Pd/C, H_2, rt, 81 %; (g) R-COOH, HATU, DIPEA, DCM, 0 °C to rt; (h) $NH_2OH \cdot HCl$, NMM, MeOH, rt; (i) Pd/C, H_2, AcOH, 50 psi, 50 °C.

attached to C-3 (H-3) and the nitrile carbon (C-8) is present while correlation between the H-3 and the methyl carbon (C-6) was not observed. Interestingly, no C-3 substituted product was formed, indicating that C-4 is more electrophilic and thus more prone to palladium insertion during the oxidative addition step. Subsequent steps involving free-radical bromination of the 5-methyl group, azide substitution, and azide reduction led to the desired intermediate **7**, which features a primary amine functional group for conjugation with a small collection of commercially available carboxylic acids.

Using intermediate **7**, molecular functionalities (R-) were easily introduced at the C-5 position of the thiophene core through amide coupling. Subsequently, the C-2 nitrile was converted into the desired amidine via reduction of an amidoxime intermediate.[20] In contrast to the conventional Pinner reaction, which requires the use of excessive gaseous hydrochloride under anhydrous conditions, this method involved the reduction of an amidoxime intermediate in acetic acid (AcOH) media under pressure (H_2) and heat (Parr reactor, 50 psi, 50 °C). Using this method, we successfully synthesized seven closely related analogues, as illustrated in Scheme 1.

The seven analogues in this study were equipped with hydrophobic rings, mainly fused heterocycles, as side chains to facilitate interactions with the +1 valine of ERα.[19b,21] The analogues were categorized into four groups based on the ring types of the side chains. Group 1 consisted of compounds **11**, **12**, and **13**, which feature the extension of benzo-fused five-membered rings. **11** and **12** are regioisomers that both contain dihydrobenzofuran rings. Indole derivative **13** is intended to be an isostere of **11**. Compounds **14** and **15** belonged to Group 2 and have an additional methylene group between the amide and the fused heterocycles, adding one additional rotatable bond to the side chains. Group 3 and Group 4 contained single specimens, **16** and **17**, respectively. Compound **16** has a reversed bicyclic ring geometry compared to **11**, while **17** has a non-aromatic oxepane ring.

Stabilization analysis and SAR on the 14-3-3/ERα complex

The stabilization effect and structure-activity relationship (SAR) of the seven analogues were investigated using fluorescence anisotropy (FA) assays coupled with X-ray crystallography analysis. Compound **11** was titrated to 100 nM fluorescein-labelled ERα peptide in the absence or presence of 1.5 μM 14-3-3σ, a concentration regime at which approximately 20 % of the ERα peptide is bound to 14-3-3σ (Figure S2A). In the absence of 14-3-3σ, no significant effect on the FA of the ERα peptide was observed at compound concentrations up to 500 μM (Figure 2A), indicating that compound **11** does not bind to the peptide alone. In contrast, when compound **11** was titrated to the mixture of ERα and 14-3-3σ, an increase in anisotropy was observed, suggesting enhanced binding of ERα to 14-3-3σ induced by **11**. Notably, a complete sigmoidal curve was not reached at these compound concentrations. To further assess the stabilizing capacity of **11** a protein titration was performed. Here, 14-3-3σ was titrated to a solution containing the ERα peptide, either in the absence or presence of compound **11**. The binding curve of 14-3-3σ to ERα showed a 6-fold enhancement in the apparent dissociation constant (Kd_{app}) in the presence of 500 μM of compound **11** (Figure 2B). This fold-enhancement is defined as the stabilization factor (SF). To confirm the activity of compound **11** on other 14-3-3 isoforms, 14-3-3η protein was used. We observed a stabilization factor of 7 for the 14-3-3η isoform, consistent with 14-3-3σ (Figure S2B). Analogously, the stabilization factors (SFs) of all the other analogues were determined to infer SAR insights (Figure 2C, Figure S3 and S4).

Analysis of the stabilization factors of all the analogues highlighted the importance of an aromatic structure and the number of rotatable bonds in the side chains. Compared to the aromatic side chain, the presence of a non-aromatic side chain led to lower stabilization factors as demonstrated by the almost inactive compound **17** (SF = 1.4-fold). Out of the aromatic side chains from group 1, the dihydrobenzofuran and indole exhibited stabilization factors ranging from approximately 6-

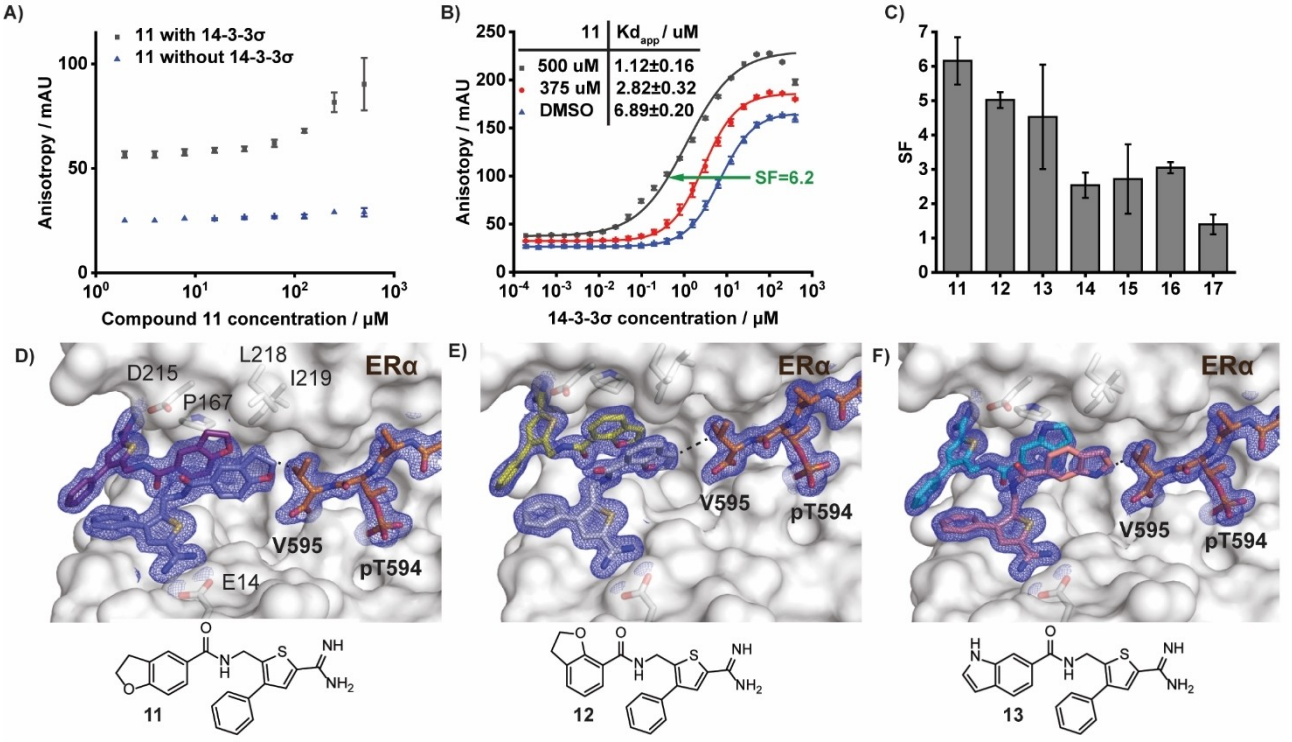

Figure 2. Stabilization of 14-3-3/ERα complex by amidine analogues and structure-activity relationship (SAR). Fluorescence anisotropy data of titrating (A) **11** to 14-3-3σ (1.5 μM) and ERα-FITC (100 nM), (B) 14-3-3σ to ERα-FITC (100 nM) in the presence of **11** (375 and 500 μM), and (C) Stabilization factors (SFs) induced by the analogues (500 μM) towards 14-3-3σ/ERα-FITC complex. (D–F) X-ray crystal structures of 14-3-3σ (white surface) and ERα (orange sticks) in presence of compounds **11**, **12**, and **13**. PDB: 7OPW, 7OQ7, and 7OQ8, respectively. All $2F_O$-F_C electron density maps are shown as blue mesh at 1σ. The two stacking molecules of each analogue are depicted as sticks and in different colors to distinguish them.

fold to 4-fold, with the 2,3-fused dihydrobenzofuran being the best (**11**, SF = 6.2-fold). In terms of group 2, a drop in stabilization factor by around a half was observed (**14** and **15**, SF = 2.5 and 2.7-fold respectively) compared to group 1, revealing a negative impact of the rotatable bond introduced by an additional methylene group. A similar trend was observed for the group 3 analogue **16** (SF = 3.1-fold), where the ring geometry is inversed.

To gain insight into the molecular mechanism underlying the observed stabilization factors, we performed X-ray crystallography analysis on co-crystals of 14-3-3σΔC/ERα soaked with all the analogues. Analysis of the structures in the presence of compounds **11**, **12**, or **13** revealed clear electron density at the Glu14 amidine-binding site (Figure 2D–F), highlighting the anchoring effect of the Glu14-amidine electrostatic interaction, in line with the initial fragment (Figure 1B). The generally termed FC-binding pocket,[10,22] which was previously unaddressed by fragment **AZ-017**,[18c] is now occupied by the additionally introduced aromatic side chains. Interestingly, a second molecule of each compound was observed within the same binding pocket. In addition, an intermolecular π–π stacking forms between the aromatic side chains of the **11**, **12**, or **13** pairs, in an off-set conformation. The side chains of these compounds also engage in hydrophobic contacts with the Pro167, Leu218, and Ile219 on the roof of the 14-3-3 binding channel. In addition, the side chains of **11**, **12** and **13** also make hydrophobic contacts with Val595 of ERα. These direct contacts with ERα provide an explanation for the enhanced stabilization relative to other analogues.

The density maps of the 14-3-3σΔC/ERα co-crystals with compounds **14** and **15** showed coverage of the Glu14-amidine electrostatic interaction (Figure S5). However, the overall occupancy of the molecular structures was low including the side chains, suggesting a higher flexibility of compounds **14** and **15**. Moreover, neither binding of a second molecule nor intermolecular π–π stacking was observed for compounds **14** and **15**, which is likely a result of the increased flexibility introduced by the additional methylene group. The inability of two-fold binding to the PPI pocket by **14** and **15** thus highlights the importance of the π–π stacking by the **11**, **12**, and **13** pairs in effectively "filling-up" the composite PPI pocket. The additional methylene group in the side chains of **14** and **15** thus leads to monovalent binding and less optimal stabilization of the 14-3-3/ERα interaction. Compounds **16** (featuring a reversed dihydrobenzofuran ring) and **17** (featuring a non-aromatic oxepane ring) also displayed weak electron density in the 14-3-3σΔC/ERα co-crystal structure (Figure S5). The increased flexibility of these side chains appears to be associated with an unfavorable entropy for binding and/or less optimal cooperativity for PPI stabilization, as demonstrated by the reduced stabilization activity of these compounds towards the 14-3-3/ERα complex.

Selectivity analysis using representative 14-3-3 binding epitopes

The FA measurements revealed compound **11** to be the most potent stabilizer for 14-3-3/ERα complex. To explore the molecular recognition within different composite pockets formed at the 14-3-3/client interface, compound **11** was screened against four other phosphopeptides, representative of a variety of 14-3-3 binding epitopes (Figure 3A, B). All the peptides contain a phosphorylated Ser or Thr, which is accommodated by the phospho-binding site formed by Lys49, Arg56, Arg139, and Tyr130 of 14-3-3. The p27 peptide has the shortest sequence with the phosphorylated Thr198 as C-terminal amino acid; The Amot-p130 and Pin-1 peptides feature respectively a polar (Glu175) or a hydrophobic (Trp73) amino acid at the +1 position relative to the phosphorylated site; The Notch-4 peptide has a sharp U-turn after the +3 amino acid.

Fluorescein-labelled p27, Amot-p130, Pin-1, and Notch-4 peptides were used in an FA assay. 14-3-3η was titrated to a constant concentration of each peptide (100 nM) in the absence or presence of 500 μM of compound **11** (Figure S6). 14-3-3η was chosen for this biophysical evaluation as it has a higher PPI affinity, enabling FA measurement with sufficient accuracy also for relatively weaker binding peptides. The absence of auto-fluorescence and non-specific binding of compound **11** toward each peptide was confirmed (Figure S6A). The FA data showed that compound **11** exhibited weak to no stabilization for the 14-3-3 PPIs involving p27, Amot-p130, Pin-1 and Notch-4, relative to ERα (Figure 3C and S6B–E).

To elucidate the molecular mechanism behind these observations, we also conducted X-ray crystallography analysis on binary co-crystals of all the aforementioned complexes soaked with compound **11**. Comparison of the binding poses of **11** among all the crystal structures revealed different modes of interactions between the side chain of **11** and the peptides

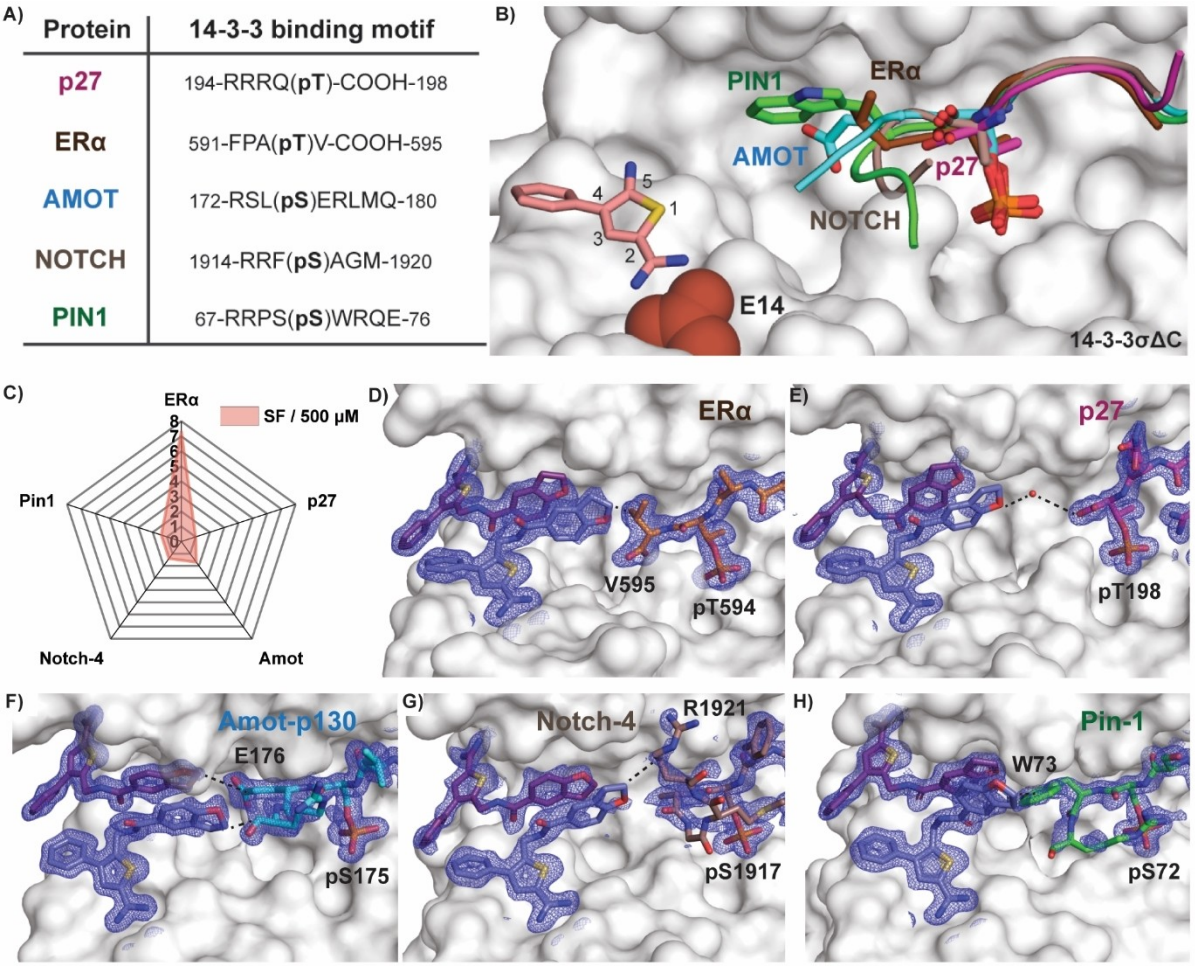

Figure 3. Selectivity profile of compound **11**. (A) Overview of the 14-3-3 binding motifs used in the study. The names and binding sequences observed in the protein/peptide complexes are reported in the table. (B) Crystallographic alignment of the binding motifs (colored cartoons) used in the study. The phospho-site and the +1 amino acids after the phosphorylation site are highlighted with stick representation. The anchoring point for the amidine group (Glu14) is represented with red spheres. 14-3-3σ is depicted with white surface. The **AZ017** fragment is represented with pink sticks (PDB: 6SIO). (C) Radar chart of the stabilization factors (SFs) induced by **11** (500 μM) against ERα, p27, Amot-p130, Notch-4 and Pin-1 peptides. (D–H) X-ray crystal structures of compound **11** bound to 14-3-3σ (white surface) and ERα (D, orange sticks, PDB: 7OPW) (see also Figure 2D), p27 (E, rose red sticks, PDB: 7OR8), Amot-p130 (F, Cyan sticks, PDB: 7OQG), Notch-4 (G, Pale Ochre sticks, PDB: 7OR3), and Pin-1 (H, green sticks, PDB: 7OQ9). All $2F_O$-F_C electron density maps are shown as blue mesh at 1σ. The two stacking molecules of **11** are depicted as blue and purple sticks respectively to distinguish them.

(Figure 3D–H). In the case of the p27 peptide, a water-mediated hydrogen bonding was observed between **11** and the distant C-terminal acid of p27 (Figure 3E). As the water bridge is probably a mere result of crystallization, the large distance between **11** and p27 explains the absence of a stabilization effect (SF = 1). For the other three phosphopeptides, direct interactions with **11** were observed. In the case of Amot-p130, one of the two molecules of compound **11** has an interaction with the backbone of the peptide and the other molecule is in proximity to the Glu176 residue (Figure 3F). Interestingly, lower occupancy of the side chain of compound **11** was observed in the crystal structures with Notch-4 and Pin-1 (Figure 3G–H). As a result, the interactions between **11** and the two peptides are less clear. In the case of Notch-4, the aliphatic part of the Arg1921 side chain appears to interact with one of the two molecules of compound **11** (Figure 3G). In the case of Pin-1, a shift in the electron density of the side chain of compound **11** was observed, suggesting a conformational rearrangement induced by the bulky Trp73 at the +1 position of Pin-1 (Figure 3H). This rearranged conformation of the side chain of compound **11** is accommodated within the composite pocket and makes hydrophobic interactions with the Trp73 residue of Pin-1, resulting in a weak effect on the 14-3-3/Pin-1 complex (SF = 1.4).

Conclusions

We have applied a fragment extension approach as a conceptual basis for the development of non-covalent 14-3-3 PPI stabilizers. Starting from the hit fragment 5-methyl-4-phenylthiophene-2-amidine (**AZ-017**), we constructed a focused library by introducing hydrophobic rings at position 5 of the thiophene core. Through fluorescence anisotropy (FA) assays, the stabilization effect of the analogues was evaluated, which identified stabilizers that enhance the affinity of the 14-3-3/ERα complex by several-fold. SAR analysis revealed the crucial role of paired binding of the compounds, mediated by the aromatic structures and a certain degree of rigidity in the side chains of the analogues. X-ray crystallography studies disclosed important interactions including hydrophobic contacts between the side chains of the analogues and C-terminal Val595 of ERα, as well as electrostatic interaction between the amidine group of the analogues and Glu14 of 14-3-3. The unique intermolecular π–π stacking binding mode of the most active analogues enables the two-fold binding of the compounds and enhances the 14-3-3/ERα affinity, indicating the need to fill the composite pocket with more bulky matter than single aromatic groups. Although it is often assumed that a single small drug molecule interacts with one protein binding site, compounds binding to target proteins with higher stoichiometry can be found during drug discovery campaigns.[23] The promising selectivity for stabilizing the 14-3-3/ERα complex by **11**, over other 14-3-3 complexes involving p27, Amot, Notch and Pin-1, provides further impetus to explore chemical expansion based on these fragment-extended starting points. Overall, this study presents a first fragment-extension approach to identify Molecular Glue for 14-3-3 PPI stabilization.

Experimental Section

Synthesis of analogues

Synthesis of 3(4)-bromo-5-methylthiophene-2-carbaldehyde (**2**). **1** (7.57 g, 60 mmol) was dissolved in AcOH (50 mL), and then Br_2 (3.7 mL, 72 mmol) in AcOH (30 mL) was added dropwisely into the solution under 0 °C. The mixture was stirred under rt for 48 h. Once the reaction was complete, it was quenched by adding saturated $NaHCO_3$. The resultant mixture was extracted with EA 3 times. The organic layer was combined, dried over anhydrous $MgSO_4$ and concentrated under reduced pressure. The obtained crude material was purified via flash silica chromatography (Hexane : EA, 0–100 %) to afford isomers 2 (4.91 g, 39.9 % yield) as pale yellow solid. Experimental data collected were consistent with those in reported literatures.[24]

Synthesis of 3(4)-bromo-5-methylthiophene-2-carbonitrile (**3**). **2** (4.30 g, 21 mmol) was dissolved in acetonitrile (60 mL), then hydroxylamine hydrochloride (2.18 g, 31 mmol), CuO (83.4 mg, 1 mmol) and AcONa (2.58 g, 31 mmol) were added to the solution. The mixture was refluxed overnight. Once the reaction was complete, it was cooled to rt. Acetonitrile was removed under reduced pressure, followed by the addition of water into the resultant residue. The mixture was extracted 3 times with EA. The organic layer was combined, dried over anhydrous $MgSO_4$ and concentrated under reduced pressure. The obtained crude material was purified via flash silica chromatography (Hexane : EA, 0–100 %) to afford isomers 3 (2.90 g, 75.3 % yield) as pale yellow solid. Experimental data collected were consistent with those in reported literatures.[25]

Synthesis of 5-methyl-4-phenylthiophene-2-carbonitrile (**4**). To a Schlenk tube was added DME (26 mL), 2 M $NaCO_3$ (20 mL), **3** (2.90 g, 14 mmol), and phenylboronic acid (2.0 g, 16 mmol). The mixture was degassed with argon, and then was added Pd tetrakis (162.4 mg, 0.14 mmol). The mixture was stirred under argon at 80 °C for 5 h. Once the reaction was complete, the mixture was cooled to rt. Brine was then added, and the resultant mixture was extracted with EA 3 times. The organic layer was combined, dried over anhydrous $MgSO_4$ and concentrated under reduced pressure. The obtained crude material was purified via flash silica chromatography (Hexane : EA = 80 : 1) to afford pure product **4** (2.10 g, 59.6 % yield) as white solid. ^{1}H NMR (400 MHz, $CDCl_3$) δ 7.54 (s, 1H), 7.45 (m, 2H), 7.42–7.30 (m, 3H), 2.53 (s, 3H).

Synthesis of 5-(bromomethyl)-4-phenylthiophene-2-carbonitrile (**5**). **4** (2.10 g, 10 mmol) was dissolved in anhydrous DCE (57.1 mL), and then the solution was brought to reflux. BPO (289 mg, 1 mmol) was added, and the addition of NBS (1.83 g, 10 mmol) was quickly followed. The mixture was refluxed and stirred for 3 h. Once the reaction was complete, the reaction was cooled to rt. The cooled mixture was diluted with EA followed by the removal of solvent under reduced pressure. The crude residue was purified via flash silica chromatography (Hexane : EA = 100 : 1) to afford product **5** with minor impurity (2.27 g, ~77.5 % yield) as white solid, and then used in the next step without further purification. ^{1}H NMR (400 MHz, $CDCl_3$) δ 8.29–7.84 (m, 1H), 7.57–7.38 (m, 6H), 4.66 (s, 2H).

Synthesis of 5-(azidomethyl)-4-phenylthiophene-2-carbonitrile (**6**). **5** (2.33 g, 8 mmol) was dissolved in acetone (92 mL) and H_2O (5 mL). To the solution NaN_3 (817 mg, 12 mmol) was added. The mixture was stirred overnight. Once the reaction was complete, the mixture

was diluted with water. The mixture was extracted with EA for 3 times. The organic layer was combined, dried over anhydrous $MgSO_4$ and concentrated under reduced pressure. The product **6** (1.52 g, 76% yield) was obtained as yellowish oil without further purification. ^{1}H NMR (400 MHz, $CDCl_3$) δ 7.60 (s, 1H), 7.51–7.40 (m, 3H), 7.39–7.29 (m, 2H), 4.57 (s, 2H).

Synthesis of 5-(aminomethyl)-4-phenylthiophene-2-carbonitrile (**7**). **6** (273.2 mg, 1.13 mmol) was dissolved in methanol (20 mL) followed by the addition of Pd/C. H_2 gas was buddled through the suspension for 2 minutes. The suspension was then stirred under H_2 atmosphere (H_2 balloon) overnight. Once the reaction was complete, the suspension was filtered through celite. The filtrate was concentrated under vacuum. The obtained crude material was purified via flash silica chromatography (hexane : EA = 1 : 1) to afford product **7** (173.7 mg, 71.8% yield) as yellowish oil. ^{1}H NMR (400 MHz, $CDCl_3$) δ 7.56 (s, 1H), 7.48–7.34 (m, 3H), 7.34–7.28 (m, 2H), 4.15 (s, 2H).

Synthesis of N-((5-cyano-3-phenylthiophen-2-yl)methyl)-R-5-carboxamides (**8**). Carboxylic acid (0.54 mmol) was dissolved in DCM (7 mL). EDCI (112.7 mg, 0.59 mmol) and catalytic amount of DMAP were added to the solution under ice bath. The mixture was stirred 10 minutes prior to the addition of **7** (105.1 mg, 0.49 mmol). Then the mixture was stirred overnight at rt. Once the reaction was complete, the mixture was washed with brine 3 times. The organic layer was dried over $MgSO_4$ and concentrated under reduced pressure. The residue was purified via flash silica chromatography (Hexane : EA, 0–100%) to afford product **8**.

Synthesis of (E)-N-((5-(N′-hydroxycarbamimidoyl)-3-phenylthiophen-2-yl)methyl)-R-5-carboxamides (**9**). 8 (2.50 mmol), hydroxylamine hydrochloride (2.47 mmol, 172.2 mg) and N-methylmorpholine (2.47 mmol, 271 uL) were added in methanol (5 mL). The mixture was stirred overnight at rt. Once the reaction was complete, the solvent was removed. The obtained residue was purified via flash silica chromatography (Hexane : EA, 0–100%) to afford product **9**.

Synthesis of N-((5-carbamimidoyl-3-phenylthiophen-2-yl)methyl)-R-5-carboxamides (**10**) via H-cube flow chemistry. **9** (0.35 mmol) was dissolved in AcOH (4 mL). Then the solution was subject to H-cube (H-cube mini plus, THALESNano) flow chemistry (100 bar, 100 °C, 1 mL/min). The reaction was monitored by LCMS. Once the reaction was complete, the solvent was removed under reduced pressure. The residue was purified via preparative column: XBridge Prep OBD C18 column 19 mm×250 mm, 5 μm; mobile phase A, water (0.1% FA); mobile phase B, MeCN; flow rate, 20 mL/min; gradient, 26% B to 28% B. The product was obtained as formic salt.

Synthesis of N-((5-carbamimidoyl-3-phenylthiophen-2-yl)methyl)-R-5-carboxamides (**10**) via Parr apparatus. **9** (0.27 mmol) was dissolved in AcOH in the high-pressure reaction vessel of Parr hydrogenation apparatus followed by the addition of Pd/C (28.7 mg, 0.27 mmol). The suspension was stirred under 50 psi and 50 °C overnight. Once the reaction was complete, the mixture was filtered through celite. The filtrate was collected and concentrated under reduced pressure. The obtained residue was purified via preparative column: XBridge Prep OBD C18 column 19 mm×250 mm, 5 μm; mobile phase A, water (0.1% FA); mobile phase B, MeCN; flow rate, 20 mL/min; gradient, 35% B to 40% B. The product was obtained as formic salt.

Analytical data for all final compounds can be found in the Supporting Information.

Peptide sequences

Peptides sequences: p27-pT198 [^{187}TPKKPGLRRRQ(pT)^{198}-COOH], Erα-pT594 [^{581}KYYITGEAEGFPA(pT)V^{595}-COOH], Amot-pS175 [^{169}GHVRSL(pS)ERLMQM^{181}], Notch4-pS1917 [^{1912}RGRRF(pS)AGMRG^{1922}], Pin1-pS72 [^{61}LVKHSQSRRPS(pS)WRQEK^{77}]. Peptides were purchased from GenScript. Notch4-pS1917 peptide was synthesized in house by Dr. Sebastian Andrei.

Protein expression and purification

14-3-3σ full length, 14-3-3η full length, and 14-3-3σΔC (C-terminally truncated after T231) were expressed in BL21 (DE3) competent cells *via* a pProEX HTb plasmid. Expression was induced with 0.4 mM Isopropyl β-D-1-thiogalactopyranoside (IPTG) overnight at 18 °C. After spinning down and lysis of the expression culture, the protein was purified on a Ni^{2+}-NTA column. The His_6-tag was cleaved with Tobacco Etch Virus (TEV) protease in 1:0.05 mg ratio, after which a second nickel-affinity chromatography was performed followed by size exclusion chromatography (Superdex75) in 25 mM Hepes pH 7.5, 100 mM NaCl, 10 mM $MgCl_2$, 2 mM β-mercaptoethanol.

Fluorescence anisotropy assays

All Fluorescence Anisotropy (FA) assays were performed in technical triplicate in 10 mM Hepes pH 7.4, 150 mM NaCl, 0.1% Tween20, 100 μM β-mercaptoethanol, and 1 mg.mL^{-1} BSA with Corning black round-bottom 384 well plates and a Tecan Infinite F500 plate reader (fluorescein: excitation 485 nm, emission 535 nm). For the compound titration experiment, each compound was titrated in a 1 : 1 dilution series to a fixed concentration of protein and fluorescein-labelled peptide as described. For the protein titration experiment, protein was titrated in a 1 : 1 dilution series to a fixed concentration of each compound (375 or 500 μM) and fluorescein-labelled peptide as described. All the graphs were plotted using OriginLab2020 and apparent Kd values were derived by fitting the data into Hill1 equation.

Protein crystallization and structure elucidation

Crystals of the 14-3-3σΔC/peptides complexes were grown by mixing 14-3-3σΔC (protein concentrations 10, 12.5 or 15 mg·mL^{-1}) in a molar ratio of 1 : 2 with the different peptides, in 20 mM Hepes pH 7.5, 2 mM $MgCl_2$, and 2 mM β-mercaptoethanol, and incubated overnight at 4 °C. The complexes were then set up for crystallization trials using the sitting drop method by mixing each complex 1 : 1 with different precipitation buffers. The precipitation buffers contained 0.095 M Hepes, PEG 400, 0.19 M $CaCl_2$, and 5% Glycerol with varying pH values (ranging from 7.1 to 7.7) and PEG 400 concentrations (ranging from 24 to 29%). Crystals were grown within 7 days and could be directly flash-frozen in liquid nitrogen. For the soaking experiments, 100 mM stock solutions in DMSO of the compounds were added to the crystals to a final concentration of 10 mM. Crystals were harvested after 11–13 days of incubation and directly flash cooled in liquid nitrogen. Data collection was performed in-house on a Rigaku MicroMaz-003 (Rigaku Europe, Kemsing Sevenoaks, UK) sealed tube X-ray source and a Rigaku Dectris PILATUS 200 K detector (DECTRIS Ltd., Baden-Daettwil, Switzerland). Data were processed using Dials.[26] Molecular replacement was carried out using Phaser.[27] The obtained model was subjected to reiterative rounds of model building and refinement using Coot[28] and Phenix.[29] Figures were prepared using Pymol software.

Supporting Information

Experimental procedures and additional data, as well as all the structures and analytical data of the molecules described in this article, are provided in the Supporting Information.[24–25]

Acknowledgements

We thank Joost L. J. van Dongen for HR-MS measurements. This research was supported by the European Union through ERC Advanced Grant PPI-Glue (101098234), Initial Training Network TASPPI, funded by the H2020 Marie Curie Actions (Grant Agreement 675179), through a Eurotech Postdoctoral Fellow program (Marie Skłodowska-Curie Co-funded, grant number 754462), the Netherlands Organization for Scientific Research via NWO Veni VI.Veni.212.27, and a China Scholarship Council PhD fellowship (CSC 201906050031). Views and opinions expressed are however those of the authors only and do not necessarily reflect those of the European Union or the European Research Council. Neither the European Union nor the granting authority can be held responsible for them.

Conflict of Interests

Christian Ottman and Luc Brunsveld are both co-founders of Ambagon Therapeutics. Christian Ottmann is currently employee and Luc Brunsveld is currently advisor of Ambagon Therapeutics.

Data Availability Statement

The data that support the findings of this study are available in the supplementary material of this article.

Keywords: 14-3-3 · Erα · Fragment · Molecular Glue · PPI Stabilizer

[1] D. E. Scott, A. R. Bayly, C. Abell, J. Skidmore, *Nat. Rev. Drug Discovery* **2016**, *15*, 533–550.
[2] Z. Z. Wang, X. X. Shi, G. Y. Huang, G. F. Hao, G. F. Yang, *Trends Biochem. Sci.* **2023**, *48*, 539–552.
[3] a) S. A. Andrei, E. Sijbesma, M. Hann, J. Davis, G. O'Mahony, M. W. D. Perry, A. Karawajczyk, J. Eickhoff, L. Brunsveld, R. G. Doveston, L. G. Milroy, C. Ottmann, *Expert Opin. Drug Discovery* **2017**, *12*, 925–940; b) L. Mabonga, A. P. Kappo, *Biophys. Rev. Lett.* **2019**, *11*, 559–581.
[4] A. J. Souers, J. D. Leverson, E. R. Boghaert, S. L. Ackler, N. D. Catron, J. Chen, B. D. Dayton, H. Ding, S. H. Enschede, W. J. Fairbrother, D. C. Huang, S. G. Hymowitz, S. Jin, S. L. Khaw, P. J. Kovar, L. T. Lam, J. Lee, H. L. Maecker, K. C. Marsh, K. D. Mason, M. J. Mitten, P. M. Nimmer, A. Oleksijew, C. H. Park, C. M. Park, D. C. Phillips, A. W. Roberts, D. Sampath, J. F. Seymour, M. L. Smith, G. M. Sullivan, S. K. Tahir, C. Tse, M. D. Wendt, Y. Xiao, J. C. Xue, H. Zhang, R. A. Humerickhouse, S. H. Rosenberg, S. W. Elmore, *Nat. Med.* **2013**, *19*, 202–208.
[5] S. L. Schreiber, *Cell* **2021**, *184*, 3–9.
[6] a) C. Maniaci, A. Ciulli, *Curr. Opin. Chem. Biol.* **2019**, *52*, 145–156; b) B. Z. Stanton, E. J. Chory, G. R. Crabtree, *Science* **2018**, *359*, eaao5902.
[7] a) J. A. Dewey, C. Delalande, S. A. Azizi, V. Lu, D. Antonopoulos, G. Babnigg, *J. Med. Chem.* **2023**, *66*, 9278–9296; b) L. G. Milroy, T. N. Grossmann, S. Hennig, L. Brunsveld, C. Ottmann, *Chem. Rev.* **2014**, *114*, 4695–4748.
[8] L. G. Milroy, L. Brunsveld, C. Ottmann, *ACS Chem. Biol.* **2013**, *8*, 27–35.
[9] I. J. De Vries-van Leeuwen, D. da Costa Pereira, K. D. Flach, S. R. Piersma, C. Haase, D. Bier, Z. Yalcin, R. Michalides, K. A. Feenstra, C. R. Jimenez, T. F. de Greef, L. Brunsveld, C. Ottmann, W. Zwart, A. H. de Boer, *Proc. Natl. Acad. Sci. USA* **2013**, *110*, 8894–8899.
[10] C. Anders, Y. Higuchi, K. Koschinsky, M. Bartel, B. Schumacher, P. Thiel, H. Nitta, R. Preisig-Muller, G. Schlichthorl, V. Renigunta, J. Ohkanda, J. Daut, N. Kato, C. Ottmann, *Chem. Biol.* **2013**, *20*, 583–593.
[11] L. M. Stevers, C. V. Lam, S. F. Leysen, F. A. Meijer, D. S. van Scheppingen, R. M. de Vries, G. W. Carlile, L. G. Milroy, D. Y. Thomas, L. Brunsveld, C. Ottmann, *Proc. Natl. Acad. Sci. USA* **2016**, *113*, E1152–1161.
[12] M. Wolter, P. de Vink, J. F. Neves, S. Srdanovic, Y. Higuchi, N. Kato, A. Wilson, I. Landrieu, L. Brunsveld, C. Ottmann, *J. Am. Chem. Soc.* **2020**, *142*, 11772–11783.
[13] L. M. Stevers, E. Sijbesma, M. Botta, C. MacKintosh, T. Obsil, I. Landrieu, Y. Cau, A. J. Wilson, A. Karawajczyk, J. Eickhoff, J. Davis, M. Hann, G. O'Mahony, R. G. Doveston, L. Brunsveld, C. Ottmann, *J. Med. Chem.* **2018**, *61*, 3755–3778.
[14] a) F. Kanai, P. A. Marignani, D. Sarbassova, R. Yagi, R. A. Hall, M. Donowitz, A. Hisaminato, T. Fujiwara, Y. Ito, L. C. Cantley, M. B. Yaffe, *EMBO J.* **2000**, *19*, 6778–6791; b) B. Zhao, X. Wei, W. Li, R. S. Udan, Q. Yang, J. Kim, J. Xie, T. Ikenoue, J. Yu, L. Li, P. Zheng, K. Ye, A. Chinnaiyan, G. Halder, Z. C. Lai, K. L. Guan, *Genes Dev.* **2007**, *21*, 2747–2761.
[15] S. Rajagopalan, R. S. Sade, F. M. Townsley, A. R. Fersht, *Nucleic Acids Res.* **2010**, *38*, 893–906.
[16] E. Freed, M. Symons, S. G. Macdonald, F. McCormick, R. Ruggieri, *Science* **1994**, *265*, 1713–1716.
[17] a) C. Johnson, S. Crowther, Margaret J. Stafford, David G. Campbell, R. Toth, C. MacKintosh, *Biochem. J.* **2010**, *427*, 69–78; b) M. Uhart, D. M. Bustos, *Front. Genet.* **2014**, *5*; c) M. B. Yaffe, K. Rittinger, S. Volinia, P. R. Caron, A. Aitken, H. Leffers, S. J. Gamblin, S. J. Smerdon, L. C. Cantley, *Cell* **1997**, *91*, 961–971.
[18] a) F. Bosica, S. A. Andrei, J. F. Neves, P. Brandt, A. Gunnarsson, I. Landrieu, C. Ottmann, G. O'Mahony, *Chem. Eur. J.* **2020**, *26*, 7131–7139; b) P. J. Cossar, M. Wolter, L. van Dijck, D. Valenti, L. M. Levy, C. Ottmann, L. Brunsveld, *J. Am. Chem. Soc.* **2021**, *143*, 8454–8464; c) X. Guillory, M. Wolter, S. Leysen, J. F. Neves, A. Kuusk, S. Genet, B. Somsen, J. K. Morrow, E. Rivers, L. van Beek, J. Patel, R. Goodnow, H. Schoenherr, N. Fuller, Q. Cao, R. G. Doveston, L. Brunsveld, M. R. Arkin, P. Castaldi, H. Boyd, I. Landrieu, H. Chen, C. Ottmann, *J. Med. Chem.* **2020**, *63*, 6694–6707; d) E. Sijbesma, K. K. Hallenbeck, S. Leysen, P. J. de Vink, L. Skora, W. Jahnke, L. Brunsveld, M. R. Arkin, C. Ottmann, *J. Am. Chem. Soc.* **2019**, *141*, 3524–3531; e) M. Wolter, D. Valenti, P. J. Cossar, L. M. Levy, S. Hristeva, T. Genski, T. Hoffmann, L. Brunsveld, D. Tzalis, C. Ottmann, *Angew. Chem. Int. Ed.* **2020**, *59*, 21520–21524; f) D. N. Kenanova, E. J. Visser, J. M. Virta, E. Sijbesma, F. Centorrino, H. R. Vickery, M. Zhong, R. J. Neitz, L. Brunsveld, C. Ottmann, M. R. Arkin, *ACS Cent. Sci.* **2023**, *9*, 937–946; g) M. Falcicchio, J. A. Ward, S. Y. Chothia, J. Basran, A. Mohindra, S. Macip, P. Roversi, R. G. Doveston, *Chem. Sci.* **2021**, *12*, 12985–12992.
[19] a) J. S. Pallesen, C. C. Munier, F. Bosica, S. A. Andrei, K. Edman, A. Gunnarsson, G. La Sala, O. D. Putra, S. Srdanovic, A. J. Wilson, L. Wissler, C. Ottmann, M. W. D. Perry, G. O'Mahony, *J. Med. Chem.* **2022**, *65*, 16818–16828; b) E. Sijbesma, E. Visser, K. Plitzko, P. Thiel, L. G. Milroy, M. Kaiser, L. Brunsveld, C. Ottmann, *Nat. Commun.* **2020**, *11*, 3954; c) E. J. Visser, P. Jaishankar, E. Sijbesma, M. A. M. Pennings, E. M. F. Vandenboorn, X. Guillory, R. J. Neitz, J. Morrow, S. Dutta, A. R. Renslo, L. Brunsveld, M. R. Arkin, C. Ottmann, *Angew. Chem. Int. Ed.* **2023**, *62*, e202308004.
[20] a) U. S. Mahajan, R. R. Godinde, P. N. Mandhare, *Synth. Commun.* **2011**, *41*, 2195–2199; b) M. Sollner Dolenc, K. Nadrah, *Synlett* **2007**, *2007*, 1257–1258.
[21] E. Sijbesma, K. K. Hallenbeck, S. A. Andrei, R. R. Rust, J. M. C. Adriaans, L. Brunsveld, M. R. Arkin, C. Ottmann, *ACS Med. Chem. Lett.* **2021**, *12*, 976–982.
[22] a) J. Ohkanda, *Chem. Lett.* **2021**, *50*, 57–67; b) A. Sengupta, J. Liriano, E. A. Bienkiewicz, B. G. Miller, J. H. Frederich, *ACS Omega* **2020**, *5*, 25029–25035; c) A. Saponaro, A. Porro, A. Chaves-Sanjuan, M. Nardini, O. Rauh, G. Thiel, A. Moroni, *Plant Cell* **2017**, *29*, 2570–2580; d) S. A. Andrei, P. de Vink, E. Sijbesma, L. Han, L. Brunsveld, N. Kato, C. Ottmann, Y. Higuchi, *Angew. Chem. Int. Ed.* **2018**, *57*, 13470–13474.
[23] M. Stornaiuolo, G. E. De Kloe, P. Rucktooa, A. Fish, R. van Elk, E. S. Edink, D. Bertrand, A. B. Smit, I. J. de Esch, T. K. Sixma, *Nat. Commun.* **2013**, *4*, 1875.

[24] S. Castellanos, A. A. Vieira, B. M. Illescas, V. Sacchetti, C. Schubert, J. Moreno, D. M. Guldi, S. Hecht, N. Martin, *Angew. Chem. Int. Ed.* **2013**, *52*, 13985–13990.
[25] S. Hiroto, K. Suzuki, H. Kamiya, H. Shinokubo, *Chem. Commun.* **2011**, *47*, 7149–7151.
[26] G. Winter, D. G. Waterman, J. M. Parkhurst, A. S. Brewster, R. J. Gildea, M. Gerstel, L. Fuentes-Montero, M. Vollmar, T. Michels-Clark, I. D. Young, N. K. Sauter, G. Evans, *Acta Crystallogr. D Struct. Biol.* **2018**, *74*, 85–97.
[27] A. J. McCoy, R. W. Grosse-Kunstleve, P. D. Adams, M. D. Winn, L. C. Storoni, R. J. Read, *J. Appl. Crystallogr.* **2007**, *40*, 658–674.
[28] P. Emsley, K. Cowtan, *Acta Crystallogr. D Biol. Crystallogr.* **2004**, *60*, 2126–2132.
[29] P. D. Adams, P. V. Afonine, G. Bunkoczi, V. B. Chen, I. W. Davis, N. Echols, J. J. Headd, L. W. Hung, G. J. Kapral, R. W. Grosse-Kunstleve, A. J. McCoy, N. W. Moriarty, R. Oeffner, R. J. Read, D. C. Richardson, J. S. Richardson, T. C. Terwilliger, P. H. Zwart, *Acta Crystallogr. D Biol. Crystallogr.* **2010**, *66*, 213–221.

Manuscript received: September 17, 2023
Revised manuscript received: October 29, 2023
Accepted manuscript online: October 30, 2023
Version of record online: November 17, 2023